Available online at www.sciencedirect.com
SCIENCE DIRECT®
Journal of Nuclear Materials 323 (2003) 57–67
journal of nuclear materials
www.elsevier.com/locate/jnucmat

Luminescence properties of zirconium oxide films

H. Ken Yueh *, Brian Cox

Centre for Nuclear Engineering, University of Toronto, 184 College Street, Toronto, Ont., Canada M5S 3E4

Received 30 June 2003; accepted 5 August 2003

Abstract

Various luminescence techniques have been applied in the characterisation of the zirconium oxide film formed on the metal matrix. Our investigation shows that some alloying elements in the zirconium alloys show characteristic emissions which could be used to study their distribution in the zirconium oxide. While the origin and detailed mechanism of luminescence in the zirconium oxide system is not well established, cathodoluminescence (CL) and thermoluminescence results from this study support the theory that oxygen vacancies in complexes with impurities are responsible for the intrinsic luminescence in the oxide system. The specific oxygen vacancy and impurity complex is reported in literature as the T-defect, having an energy of 2.2 eV. To aid in interpretation of the CL data, optical transmission properties of the oxides were also measured. The latter investigation showed the thickness of the oxide illuminated by the CL technique is greatly dependent on the optical transmission properties of the oxide, and it ranges from 20 μm for pure zirconium or low-alloyed zirconium oxides to less than 3 μm for oxides of alloys with more absorbing, or higher alloying element concentrations. The 20 μm depth of illumination is significantly deeper than the electron penetration depth, which suggests a secondary source of excitation, possibly characteristic X-rays emitted by the specimen. These combined properties of the oxide and technique can result in CL images showing structural contrast not easily seen during SEM or optical microscopy of oxidised surfaces.

1. Introduction

Zirconium alloys are widely used in the cores of nuclear reactors. Their uses range from fuel cladding and pressure tubes to fuel grid spacers and garter springs. The material is mostly used after alloying with some other elements for improved performance; it lacks the required mechanical and corrosion properties in a high temperature water environment in its pure form. To meet these requirements, zirconium is usually alloyed with Sn, Nb, Fe, Cr and Ni for improved mechanical and corrosion properties. Most of the alloying elements with the exception of Sn and Nb have very low solubilities in the zirconium matrix and they end up as intermetallic precipitates; $Zr(Cr,Fe)_2$ and $Zr_2(Ni,Fe)$ in Zircaloy-2 and $Zr(Cr,Fe)_2$ in Zircaloy-4. Under irradiation conditions, these alloys show an increased oxidation rate. Investigations of this phenomenon revealed the involvement of the intermetallic precipitates; it was observed from these examinations that some of the alloying elements diffuse out of the precipitates into the metal matrix under irradiation conditions. The solubility limit of these alloying elements is generally very low, in the order of 100 parts-per-million (ppm). Existing techniques for non-destructive chemical analysis do not have the sensitivity required for their detection when in solution in the Zr matrix. Since alloying element distributions in the final oxide have an important impact on the oxidation rate of the alloy [1], it is therefore necessary to search for an alternative technique that is capable of detecting alloying elements at these low concentrations.

Luminescence techniques have the required sensitivity for this purpose; however, there is no unified quantitative theory [2]. In addition, there is no published

* Corresponding author. Tel.: +1-803-647-3836; fax: +1-803-695-3973.
E-mail address: yuehk@westinghouse.com (H.K. Yueh).

0022-3115/$ - see front matter © 2003 Elsevier B.V. All rights reserved.
doi:10.1016/j.jnucmat.2003.08.025

literature on the luminescence properties of zirconium oxide films formed from a metallic substrate, only bulk zirconia material has been studied. There are numerous publications on stabilised bulk zirconia, these reports suggest that oxygen vacancies and/or impurities are involved in the luminescence process [3–9]. One of the earliest theories attributes the luminescence in the zirconium oxide system to titanium impurity ions [10,11]. Later theories link the involvement of oxygen vacancies to the luminescence process. There are three major competing theories for the explanation of the luminescence process in the zirconium oxide system involving oxygen vacancies; these theories arise from EPR measurements. One model attributes the EPR signal to a localised energy state of Zr^{3+} ions with two nearest-neighbour oxygen vacancies in the opposite cube corners, called a T-defect [12–16], having an energy of 2.2 eV [13]. A second model attributes the signal to a Cr^{3+} ion in a sixfold pseudo-octahedral, trigonally distorted site [12], and a third model attributes the signal to a singly ionized oxygen vacancy bound to a Y ion [15], although these authors later attributed it to some unknown impurities [16]. If the luminescence signal could be linked to specific impurities, this method could be ideally suited for the study of the distribution of the alloying elements in zirconium oxide films. This paper presents the results of a preliminary study gathering luminescence data for zirconium oxide powders and zirconium oxide films formed from the zirconium alloy matrix. It is to be the hope that these results will be of help in understanding the distribution of alloying elements in oxides formed from the metallic matrix of the alloy.

2. Experimental procedure

Three sets of samples, that consisted of commonly used commercial alloys, zirconium oxide powders doped with other elements, and binary zirconium alloys especially made for this study, were used in the investigation. At the start of this study, little was known about the luminescence properties of zirconium oxide films formed on metallic substrates. One of the questions asked was whether luminescence signals emitted by the oxide film could be detected. The readily available commercial alloys, used in an earlier corrosion study [17] were used in a photoluminescence (PL) and a thermoluminescence (TL) experiment to answer the question. The results of the PL and TL experiments indicated strong luminescence signals from the test coupons, and based on the encouraging test results, a home made cathodoluminescence (CL) apparatus was constructed for emission spectra determination and imaging.

The commercial alloy samples were made up of coupons of approximately $20\times20\times1.95$ mm^3 in dimension, and were oxidised at various temperatures and in various environments. Detailed oxidation information for these samples is listed in Table 1 and their chemical analyses are listed in Table 2. A SPEX fluorolog 212 spectrometer was used for the PL experiments. A 150 W xenon bulb provided the excitation energy. Small sections of some of these coupons were cut into 3×3 mm^2 pieces and ground to 1 mm thickness for TL measurements. The TL glow curves were obtained by exciting the samples with UV light for one minute duration (55 mW/cm^2 at 254 nm) with a 10 min waiting period before each measurement. A Teledyne TLD7300 thermoluminescence dosimeter reader was used to obtain glow curves. The samples were heated at 4.4 and 9.2 K/s.

High purity binary zirconium oxide powders were prepared to evaluate dopant CL emission characteristics. The powders were produced using a co-precipitation method and doped with various elements at concentrations of 1000–10 000 ppm by weight. The base zirconyl nitrate hydrate had a purity of 99.99%. Powders of the various elements in the form of nitrates or chlorides were dissolved in water and precipitated with ammonium hydroxide. The solutions were then boiled dry,

Table 1
List of materials used in the PL and TL study [17]

Sample	Alloy type	Oxidation condition	Oxide thickness (m)
Be5	High purity Zr	673 K steam	16
Be150	High purity Zr	573 K fused salt	1.5
Bh14	Zircaloy-2	673 K steam	1
Ac838	Zircaloy-2	773 K steam	11
E51	Zr–2.5%Nb	573 K air	12
Aw143	Zr–2.5%Nb	873 K steam	16
Aw155	Zr–2.5%Nb	873 K steam	16
Aw273	Zr–2.5%Nb	573 K air	2.6
Aw278	Zr–2.5%Nb	573 K steam	2.6
Bb3	Zr–0.5%Cu–0.5%Mo	873 K steam	5
Bb5	Zr–0.5%Cu–0.5%Mo	673 K steam	10

Table 2
List of alloying elements and major impurities

Alloy	Batch	Sn wt%	Nb wt%	Fe wt%	Cr wt%	Ni wt%	Cu wt%	Mo wt%	O wt%	Hf wt. ppm	Ti wt. ppm
Zr	Be	<0.02	<0.01	0.008	0.002	<0.001	<0.0025	<0.001	50	75	<20
Zircaloy-2	Bh	1.45	<0.01	0.14	0.09	0.05	<0.002	<0.001	1000	60	<20
	Ac	1.53	–	0.12	0.1	0.06	0.003	<0.001	1150	51	46
Zr–2.5%Nb	E	–	2.55	0.0305	<0.003	0.0025	–	–	1220	<50	50
	Aw	–	2.7	0.096	0.0025	0.004	0.004	–	1050	67	20
ATR[a]	Bb	–	–	0.03	<0.003	<0.01	0.5	0.55	800	<200	<100

[a] Zr–0.5%Cu–0.5%Mo.

and the precipitates were collected and crushed in an alumina crucible. The fine powder precipitates were heated at 1273 K for 1 h in air and were mounted on double-sided sticky tape for examination under the scanning electron microscope (SEM).

In addition to the high purity oxide powders, small buttons of the binary alloys of zirconium with various elements of interest were made using a non-consumable tungsten arc furnace at concentrations of 0.1% and 0.5% by weight. The base zirconium metal, 99.94% pure, in the form of thin sheet was used as the starting material. The alloys were made by wrapping the zirconium foil around the dopant, and melting it in the arc furnace. Each sample was flipped and remelted four times before removal from the arc furnace for further processing. The resultant alloys took the form of flattened spherical buttons. To facilitate cutting, the buttons were flattened further in a hydraulic press and cut with a diamond impregnated disk saw into smaller pieces. The smaller pieces were then flattened again into thin (1–2 mm thick) sheets before being vacuum sealed inside a fused silica tube for annealing. Samples were annealed for 24 h at 1273 K and were allowed to cool in the furnace. All of the binary alloy samples were oxidised in air at 723 and 873 K. These samples were used in CL experiments only and were studied for their CL surface features as well as CL intensities as a function of oxide thickness.

A few oxidised samples, from the commercial alloy and binary alloy groups, had the optical transmission properties of their oxides measured to aid in interpretation of the CL data. These samples were prepared by first cutting small samples in the form of 3 mm diameter discs with a core tube and diamond paste from the larger samples. The discs were then ground on one side until a thickness of 120 μm was achieved. A 'liquid tape' was then applied to cover up the metal side of the disc, leaving only a small patch (1 mm^2 in area) in the centre of the sample visible to the environment. The exposed metal part was dissolved by etching in mixed nitric/hydrofluoric acids to leave a window of exposed oxide.

A Perkin–Elmer Lamda 3 UV–VIS spectrometer was used to measure the absorption/transmission properties. The instrument is capable of supplying light of a continuously variable wavelength ranging from 190 to 900 nm. Since the incident beam from the UV–VIS spectrometer was approximately 1 mm in width and 1 cm in length, a rectangular metal mask with a small hole in the centre was inserted in the incident beam to assist in the transmission measurements. It served to reduce the size of the incident beam to the dimension of the oxide window. Precise computation of the normalised transmission rate through the oxide could be calculated based on the known mask area. Before each measurement, the transmission was normalised to 100% with the metal mask in place.

A home made CL attachment was made for a Hitachi S-570 model SEM. A schematic diagram of the apparatus set up for CL imaging is shown in Fig. 1. When the apparatus is operating, electrons from the scanning beam excite other electrons in the sample into the conduction band and emit light upon its return to the

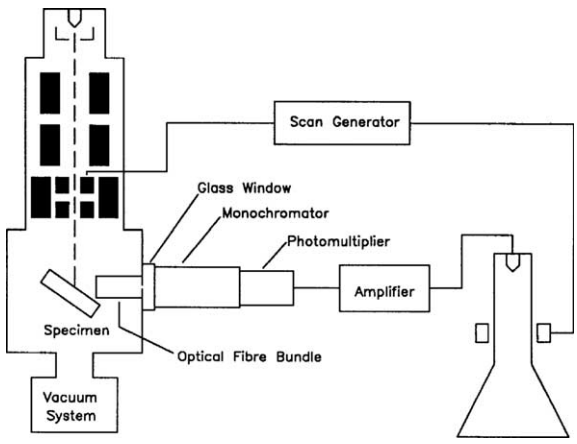

Fig. 1. Schematic diagram showing the CL configuration for imaging in the SEM.

ground state. As can be seen from the figure, light is collected via a glass fibre bundle, approximately 1.5 cm in diameter and 10 cm in length, capable of transmitting light of wavelengths from 350 to 900 nm. The transmission characteristic of the bundle is nearly constant from 370 to 900 nm, and only degrades significantly below 350 nm. The fibre bundle conducts the light emitted from the specimen to the glass window on the specimen chamber. Once the light reaches the window, it can be measured directly with a photodiode or photomultiplier. The signal from the photomultiplier can be fed back into the SEM's electronic system to generate panchromatic images. By using a monochromator between the glass window and the photomultiplier, the apparatus was capable of giving either sample emission spectra or monochromatic images. A cold stage was also built to cool the sample down with liquid nitrogen. An 1/8 in. (3.2 mm) diameter copper tube was used to transport liquid nitrogen to the specimen stage under a slight positive pressure. One end of the tube was connected to the liquid nitrogen bottle while the other end exited to the open air. Compression fittings with Teflon rings were used to seal the copper tubes at the entry points to the inside of the microscope.

3. Results and discussion

As this study represents the initial investigation of the luminescence properties of zirconium oxide without stabilisation additions, little was known and thus the study was multifaceted, involving several luminescence techniques. During the course of the investigation, several types of characterisation experiments were performed in order to interpret the data. The results and discussion are divided into four sections covering the various aspects of the study. The observed emission peaks from the PL and CL experiments on commercial alloys and binary oxide powders, representing the primary objectives of this study, are discussed first. Section 3.2 discusses the TL and CL experimental results which help to explore the effects of the alloying elements on the luminescence properties, and provide support to the discussion of the origin of the emissions presented in Section 3.3. Section 3.4 provides a discussion of the oxide optical experimental data in support of the interpretation of the CL observations.

3.1. Emission spectra

All of the samples used in the PL experiments, tabulated in Table 1, showed two emission peaks, centred around 425 and 500 nm, but only one emission peak was observed in the CL experiments, centred around 500 nm at room temperature. An example of a PL excitation and emission spectrum of a high purity zirconium sample (crystal bar Zr) oxidised in 673 K steam to an oxide thickness of 4 μm is shown in Fig. 2. However, at lower temperatures in CL experiment, the emission spectra change to reveal multiple peaks, as shown in Fig. 3 for a Zircaloy-2 sample. All of the PL spectra show a shift between the excitation and the emission spectrum (Stokes shift), i.e., the emission wavelength is longer than the excitation wavelength. In these transitions, optical absorption excites electrons to a vibrational state (where the lattice is relaxed to accommodate the electron) which is above the equilibrium electronic state. This state decays to the equilibrium electronic state with the aid of multiple phonon emissions and then returns to a vibrational ground state in a radiative transition. The difference in emission between photo-excitation and electron-excitation may be attributed to the nature of the excitation source. This means that the main paths for recombination are different for the different excitation mechanisms. This should be no surprise since the energies of the two excitation sources are vastly different relative to the band gap of the zirconium oxide. The band gap of the zirconium oxide is estimated to be in the region of 5 eV [13]. The observed absorption energy level in PL experiments is in the range of 3.5–4 eV, this is clearly below the energy required to excite electrons directly into the conduction band. In contrast, the excitation energy in CL experiments is of the order of 20 keV, many orders of magnitude higher than that needed to excite electrons directly to the conduction band. It is possible therefore that the radiative recombination of excited electrons may take different paths. The dominance of the emission peak centred around 500 nm at room temperature in CL experiments suggests that different excitation conditions may favour different recombination paths. The phenomenon of recombination path saturation under electron excitation, in which alternative recombination paths are followed by electrons once the primary one has saturated, is well documented [18,19]. There is also a slight shift in peak locations between photon and electron excitation. This may be due to the penetration differences between the excitation energy sources.

It is worthwhile mentioning the effect of temperature on the CL emission spectra, which is also illustrated in Fig. 3. When the specimen was cooled with liquid nitrogen, the CL signal strength increased dramatically. The increased signal strength allowed the use of small slits on the monochromator, which provided better spectroscopic resolution. At room temperature, some of the samples do not give a signal of sufficient strength for the use of small slits on the monochromator. This had the effect of degrading the resolution of the monochromator. The use of small slits (1 mm) improved the resolution to approximately 1 nm, which enabled two additional emission peaks at 440 and 550 nm to be resolved with the cooled Zircaloy-2 sample. The relative

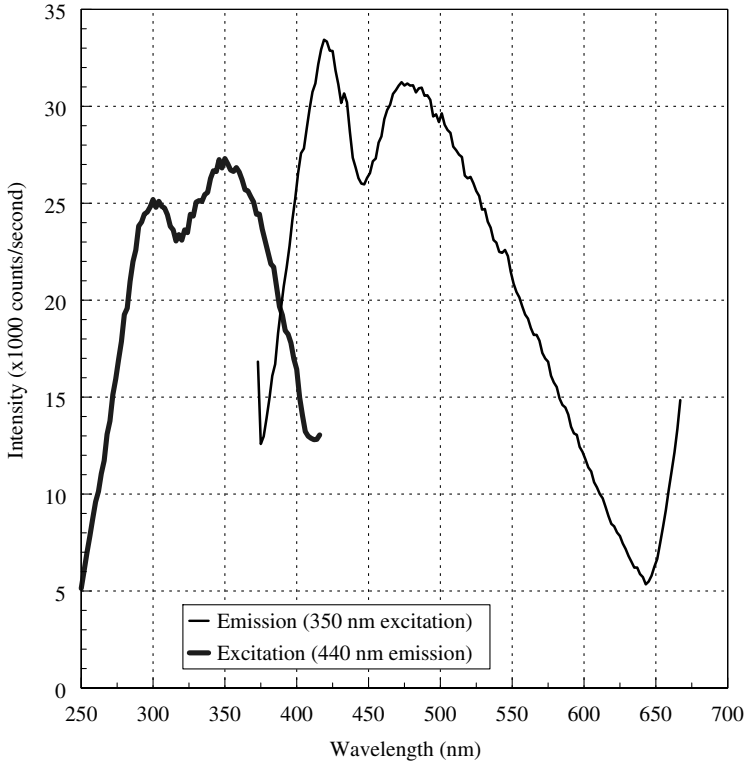

Fig. 2. PL spectra of high purity zirconium oxidised in 673 K steam, 4 μm oxide.

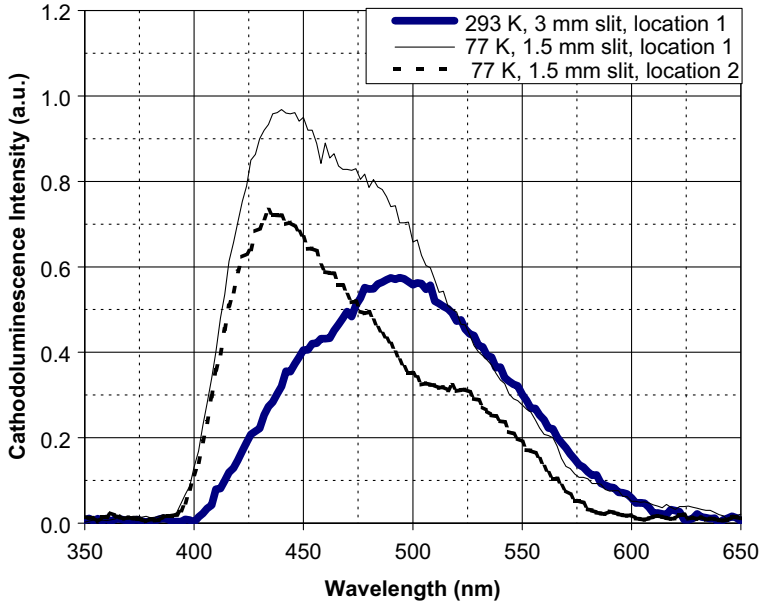

Fig. 3. CL emission spectra of Zircaloy-2 oxide film formed in 773 K steam, 11 μm oxide.

Table 3
Summary of the emission peak positions for the various dopants in zirconium oxide powders, dopant concentrations were 0.01%

Dopants	Peak 1	Peak 2	Peak 3	Peak 4
Pure Zr	485			
Sn	470			
Ni	495			
Fe	495			
Cr	450	500	550	
Ti	485			
Zn	500			
Hf	450	500		
Tb	490	550	590	630
Ce	525			
Cs	450	500	550	
Cu	500			

signal strength of the 440 nm emission peak at below room temperature would again suggest an increase in the efficiency of a second recombination path.

The absence of characteristic emission peaks with the oxidised zirconium alloy specimens at room temperature prompted the investigation of high purity binary zirconium oxide powders. Since the number of alloying and impurity elements in the common zirconium alloys is large and therefore may produce broadband emission peaks, it was hoped that by producing binary combinations of zirconium and other alloying elements/impurities, better defined emission peaks would be resolved. A summary of some of the oxide combinations that were studied and their CL emission peaks is given in Table 3. It was discouraging to find that most of the main alloying elements, with the exception of Cr, showed no characteristic emission peaks. The Zr–Cr combination, showed emission peaks at 450, 500 and 550 nm, which might be responsible for the emission peaks in the oxidised Zircaloy-2 sample when it was cooled with liquid nitrogen. Other combinations, such as the Zr–Tb system, showed unique characteristic emission peaks at 490, 550, 590 and 630 nm. These represent transitions between the inner D and F shells of the atom. A metallic sample of this binary alloy also showed distributions of Tb in the oxide matrix in CL images.

3.2. Thermoluminescence and cathodoluminescence intensities

The TL and CL signal intensities are presented to show the effect of alloying elements on luminescence. The total TL counts and CL intensities for the samples are presented in Table 4. From these numbers, it is clear that the luminescence intensity is greatly dependent on the chemical composition of the alloy. For example, it would appear that Cu or Mo greatly enhances luminescence while Nb depresses it. This therefore gave support for the hypothesis of alloying element involvement in the luminescence process.

The trap levels associated with two TL glow curves, shown in Fig. 4, were calculated and compared to those reported in literature for stabilised zirconia. The glow curves reveal two peaks, one centred around 375 K and the other at 460 K. Values of 373 and 508 K were reported in literature for bulk zirconia [20]. The difference in the peak locations may partly be due to the heating rate of 21.5 K/s used by these researchers. The trap levels were calculated using the two heating rates method and gave values of 0.30 and 0.88 eV for the 375 and 460 K peaks respectively. The 0.88 eV trap level agrees well with the literature value of 0.87 eV which corresponds to the energy level of an electron trapped at an oxygen vacancy [21]. This result then suggests similarity in luminescence property between stabilised and non-stabilised zirconia.

3.3. Origin of the emission

Establishing a link between the source luminescence and alloying/impurity elements in the zirconium oxide system is crucial to the application of the technique to the study. Although there are a number of publications available on the luminescence properties of magnesia, yttria and calcia stabilised zirconia [3,10,12,22–26], the origins and detailed mechanism of the luminescence are still not clear and are the subject of controversy. Early work assumed the origin of luminescence to be substitutional Ti^{4+} ions [3,11]. Later, structural defects such as oxygen vacancies were considered [4,5]. More recent work on the subject attributes the luminescence to oxygen vacancies in a complex with other alloying elements in the nearest-neighbour cation shell [3,6–9]. The evi-

Table 4
CL and TL intensities of the various alloys used in the preliminary study

Alloy type	Oxidation condition	Oxide thickness micrometer	CL intensity (pA)	TL intensity (counts)
High purity Zr	673 K steam	16	200	116 738
Zircaloy-2 (Ac)	673 K steam	11	250	917
Zr–2.5%Nb (Aw)	673 K steam	16	63	613
Zr–0.5%Cu–0.5%Mo	673 K steam	10	700	341 008

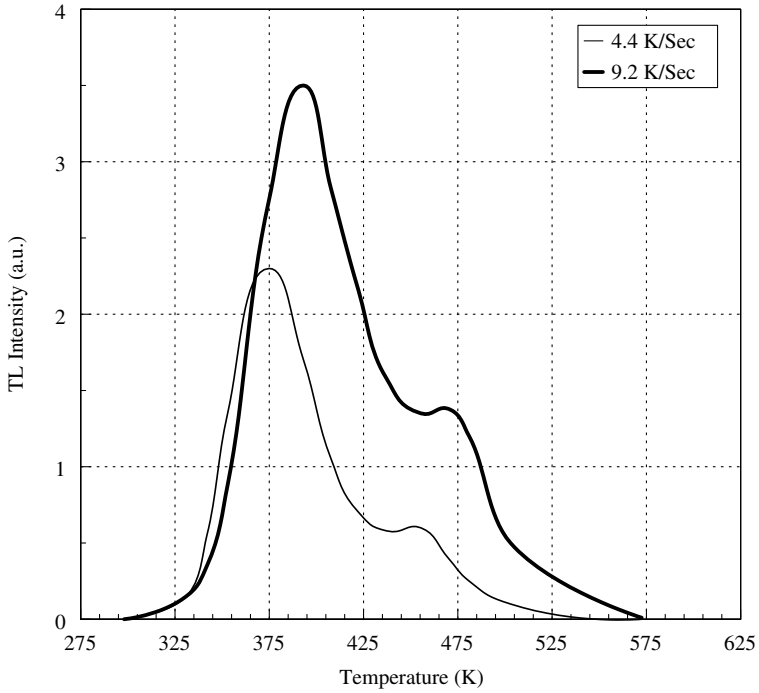

Fig. 4. TL glow curves for high purity Zr oxidised in 673 K, 16.1 μm oxide.

dence from this study supports the last of the three scenarios. Even though Ti doped zirconium samples showed extremely high luminescence signals in the oxide powder experiments, other dopants such as Cu also produced high luminescence signals. This observation disproves the theory that Ti^{4+} impurity ions are the sole origin of the luminescence. Oxidation of zirconium alloys starts initially at the metal/environment interface, and the process is controlled by the inward diffusion of oxygen from the oxide/environment interface to the metal/oxide interface. As the oxide thickens, variation in oxygen potential is developed across the oxide, resulting in an increasing mobile oxygen vacancy concentration toward the metal/oxide interface. If oxygen vacancy complexes were responsible for the luminescence then when one looks at the CL images of a section through the oxide one should see an increasing CL intensity towards the metal/oxide interface. When such a sample was produced, (Fig. 5; lower portions of part (b) and part (c)) such a distribution was not seen in the CL image. The edge-on CL image clearly showed that the origin of the luminescence in zirconium oxide did not originate from the oxygen vacancy distribution alone. There is strong evidence that it is linked to one of the other elements in the material. In general, strong luminescence signals are detected from the grain boundaries, where there is known segregation of alloying elements in specimens slow-cooled from the β-phase. This is especially clear in the Fe doped samples, shown in Fig. 5, where areas near the Zr_3Fe precipitates show extremely high CL signals. The CL images reveal structural information not clearly visible in SE images in the SEM, or in the optical microscope, and show that this technique has promise for studying the sub-structure of oxide films.

3.4. CL signal strength and attenuation

The CL signal strength as a function of the oxide thickness was recorded to characterise the oxide development as a function of time at temperature, and is plotted in Fig. 6 for a Zr–Ni alloy. The plot shows the CL signal strength continues to rise even after the oxide had reached thicknesses of more than 20 μm. This is in contradiction to the commonly known electron penetration depth of a few micrometers. So how is it that the signal continues to rise well beyond the electron penetration depth? The answer may be the possibility of a second source of excitation energy that is capable of much deeper penetration. One possible energy source is the X-rays generated during the electron bombardment. These can easily penetrate the entire oxide layer. Measurements of the optical transmission properties of zirconium oxide films indicated that zirconium oxide is quite transparent to light of about 500 nm wavelength. A plot of the fraction of the light transmitted as a

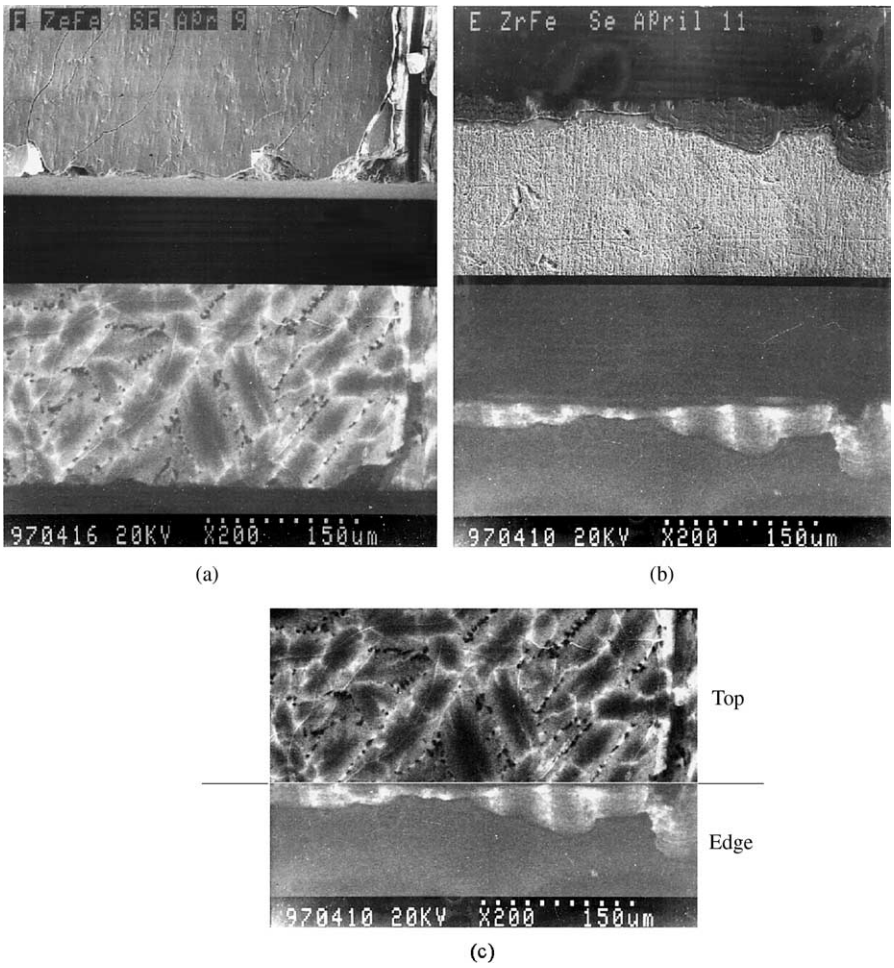

Fig. 5. SE and CL images of a Zr–0.1%Fe alloy, (a) SE and CL top view, (b) SE and CL edge view, (c) top and edge CL view matched together.

function of the oxide thickness indicated the attenuation of light is not constant for the entire thickness of the oxide. The fraction of the light transmitted decreased more slowly than expected for a linear rate as the oxide thickened. This means that there is higher attenuation for the oxide near the metal/oxide interface and that the oxide is more transparent near the oxide/environment interface. This is supported by higher calculated absorption coefficients of thin oxides. The decrease in the absorption coefficient for thicker oxides means that the oxides grown below the top layers (i.e., near the metal/oxide interface) are less transparent to light than the outer oxide layers. This is consistent with the common observation that thin (2 μm) pre-transition oxides are generally black, and that thick white post-transition oxides usually show a dark band near the oxide–metal interface in the optical microscope. Even for oxides thicker than 10 μm, more than 4.9% of the light generated internally is still transmitted to the outside. This transmission depth would be increased for very thick oxides since these would be more transparent on average than thinner oxides. Experimental data indicated that the CL signal quickly saturated when the oxide had exceeded a thickness of 20 μm for dilute alloys.

One other observation which should be noted here is that when comparing CL signal strengths, the absolute value of the CL signal does not necessarily give the true luminescence strength of the material unless the transmission properties of the oxide are considered. This is evident in the CL measurements of the Zr–0.5%Cu–0.5%Mo (ATR) alloy shown in Fig. 7. This graph plots the CL intensities for two groups of specimens of this alloy oxidised at 773 and 873 K in steam. The data shown here reveal that higher oxidation temperatures produced higher CL signal strengths and that the CL signal saturates after an oxide thickness of only 3 μm.

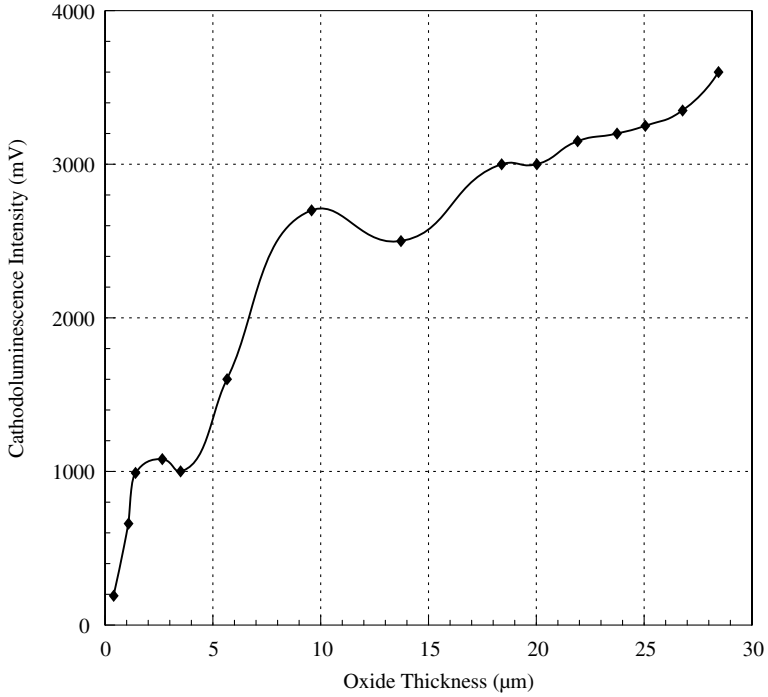

Fig. 6. Plot showing CL emission intensity vs. oxide thickness for a Zr–0.1%Ni alloy contaminated by Cu, oxidised in 723 K air.

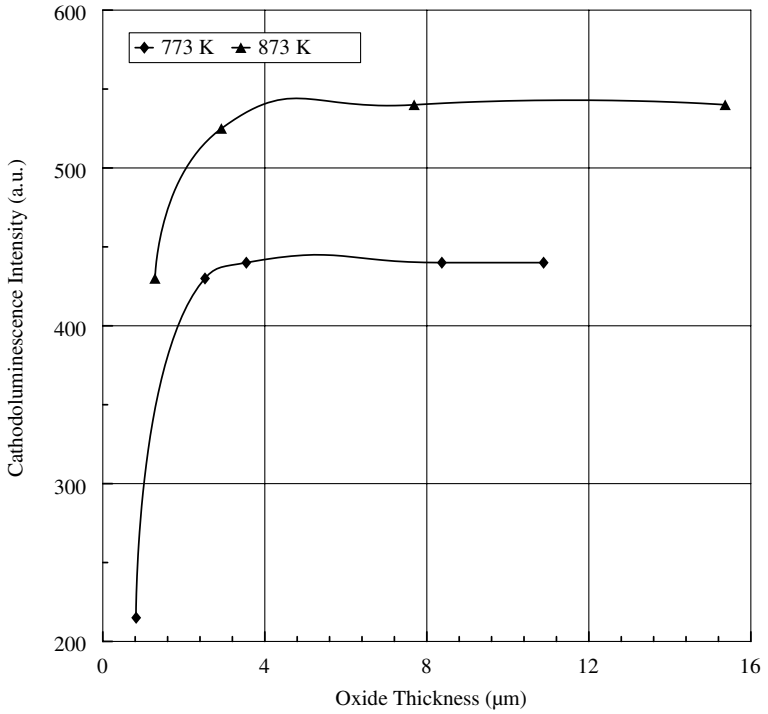

Fig. 7. CL intensity vs. oxide thickness of Zr–0.5%Cu–0.5%Mo (batch Bb, Table 2) alloy at different oxidation temperatures.

Table 5
Table showing the optical transmission properties of the various oxides samples

Alloy	Oxide thickness (μm)	Oxidation temperature (K)	Transmission (%)	
			500 nm	800 nm
Pure Zr (99.994%)	2	873	8.0	25.6
	6.3	873	3.2	13.5
	10.7	873	1.4	4.9
	2	723	3.5	14.1
	2.5[a]	723	4.5	19.0
Zr–0.5%Cu–0.5%Mo	2.9	873	1.1	3.65
	7.7	873	0.1	0.75
Zircaloy-2 (Ac)	3.8	873	0.1	0.4
	5[a]	873	0.3	0.8

[a] Sample was beta annealed before oxidation.

The saturation after 3 μm can be explained by looking at the transmission data for the oxide on this alloy. The transmission of this material is only 3.5% at a wavelength of 800 nm and slightly over 1% at 500 nm for an oxide of only 3 μm thick, and this drops to 0.75% and 0.1% respectively when the oxide is 7.7 μm thick. Linear optical absorption coefficients of 0.35 and 0.15 for the Zr–0.5%Cu–0.5%Mo and pure zirconium oxide respectively were calculated at the 800 nm wavelength. The higher absorption coefficient for the Zr–0.5%Cu–0.5%Mo clearly explains the lower transmission for the oxide on this alloy. For other alloys oxides with lower optical attenuations, the CL emission signal increased with oxide film thickness. A summary of the transmission characteristics of the oxides examined in this study at 500 and 800 nm is provided in Table 5. Any CL examination of the Zr–Cu–Mo alloy would only be able to measure the characteristics of the top 3 μm of the oxide film. This finding then would suggest that there is very little change in the CL emission characteristics as the oxide on this alloy thickens, i.e., the CL signal intensity from the top layer of the oxide does not change over time as the alloy continues to oxidise. This is true provided that the growing oxide remains intact. A set of Zircaloy-2 samples was oxidised at 873 K, and some of the samples had large amounts of oxide spall off. The optical transmission characteristics of this material are very similar to those of the Zr–Cu–Mo alloy; they both have very low transmission, but the CL emission curves look different, the intensity actually reaches a plateau and then decreases for the Zircaloy-2 samples. This would indicate that the properties of the top layer have changed somehow. Examinations showed that the oxides at the surface of these samples were severely cracked and that many pieces had fallen off. The plateau on the emission curve may be explained by the high emission intensities from areas where the oxide had fallen off. Later on, after further oxidation, this high CL signal faded indicating that chemical changes were taking place, possibly Fe diffusing out to the surface [27,28] to form Fe_2O_3 which is not luminescent.

4. Conclusions

The preliminary luminescence results presented here clearly show that this technique could be a useful tool in the investigation of the distribution of low concentration alloying elements in the zirconium oxide system. The work presented here is a first step in information gathering on the luminescence and optical properties of zirconium oxide films grown on an alloy substrate. The survey of the oxide systems has revealed several dopants (e.g., Cr, Cs, Tb) that emit characteristic signals. The CL images from oxidised alloys contain structural information on the oxide films that is not visible in SE or optical images of the same oxide. Although the present CL apparatus does not have the required light gathering efficiency to fully investigate these characteristic signals, further work is recommended to fully exploit these luminescence techniques.

Acknowledgements

The use of the PL spectrometer and advice by Professor M. Winnick (University of Toronto, Chemistry Department), and of the TL reader by Dr B. Heinmiller (Chalk River Laboratory) is gratefully acknowledged. Discussions with Professor H. Ruda (Department of Metals and Materials Engineering) during the course of these studies were very helpful.

References

[1] Waterside Corrosion of Zirconium Alloys in Nuclear Power Plants, IAEA-TECDOC-996, IAEA, Vienna, 1998.

[2] B.G. Yacobi, D.B. Holt, Cathodoluminescence Microscopy of Inorganic Solids, Plenum, New York, NY, 1990.
[3] S.E. Paje, M.A. Garcia, J. Llopis, M.J. Saavedra, C. Parada, Phys. Stat. Sol. (a) 148 (1995) K45.
[4] P.A. Arsenev, K.S. Bagdasarov, A. Niklas, A.D. Ryazantsev, Phys. Stat. Sol. 62 (1980) 395.
[5] E.D. Wachsman, N. Jiang, C.W. Frank, D.M. Mason, D.A. Stevenson, Appl. Phys. A 50 (1990) 545.
[6] S.E. Paje, J. Llopis, Appl. Phys. A 55 (1992) 523.
[7] V.R. PaiVerneker, A.N. Petelin, F.J. Crowne, D.C. Nagle, Phys. Rev. B 40 (1989) 8555.
[8] J. Llopis, Phys. Stat. Sol. (a) 119 (1990) 661.
[9] J. Llopis, R. Vila, A. Ibarra, J. Phys. Chem. Sol. 52 (1991) 903.
[10] J.F. Sarver, J. Electrochem. Soc. 113 (1966) 124.
[11] C. Bettinali, G. Ferrariso, J.W. Manconi, J. Chem. Phys. 50 (1969) 3957.
[12] P.J. Alonso, R. Alcala, J. Casas-Gonzalez, R. Cases, V.M. Orera, J. Phys. Chem. Sol. 50 (1989) 1185.
[13] R.I. Merino, V.M. Orera, Sol. State Ion. 76 (1995) 97.
[14] V.M. Orera, R.I. Merino, Y. Chen, R. Cases, J.P. Alonso, Phys. Rev. B 42 (1990) 9782.
[15] J. Shinar, D.S. Tannhauser, B.L. Silver, Sol. State Commun. 56 (1985) 221.
[16] J. Genossar, D.S. Tannhauser, Sol. State Ion. 28–30 (1988) 503.
[17] B. Cox, R.W. Ball, A study of oxide film breakdown on zirconium alloys by capacitance measurements, Canadian Report, AECL-2144, 1964, Chalk River, Ontario.
[18] W.F. van der Weg, M.W. van Tol, Appl. Phys. Lett. 38 (9) (1981).
[19] M.V. Zamoryanskaya, A.Ya. Valters, Opt. Spectrosc. 76 (4) (1994) 546.
[20] S.C. Chang, C.S. Su, Radiat. Prot. Dosim. 47 (1993) 87.
[21] W.C. Hsieh, C.S. Su, J. Phys. D: Appl. Phys. 27 (1994) 1763.
[22] C. Bonola, P. Camagni, N. Omenetto, G. Samoggia, J. Lumin. 48&49 (1991) 797.
[23] K.M. Ganguly, S. Sarkar, S.N. Bhattacharyya, J. Chem. Soc., Chem. Commun. (1993) 682.
[24] G.M. Phatak, K. Gangadharan, H. Pal, J.P. Mittal, Bull. Mater. Sci. 17 (1994) 163.
[25] S.E. Paje, J. Llopis, Appl. Phys. A 57 (1993) 225.
[26] S.E. Paje, J. Llopis, Appl. Phys. A 59 (1994) 569.
[27] C.S. Zhang, B. Li, P.R. Norton, J. Nucl. Mater. 223 (1995) 238.
[28] C.S. Zhang, B. Li, P.R. Norton, Surf. Sci. 338 (1995) 157.